AIAA JOURNAL
Vol. 37, No. 12, December 1999

Effect of Wall on Impulse of Solid Propellant Driven Millimeter-Scale Thrusters

H. Mirels*
The Aerospace Corporation, El Segundo, California 90245-4691

An analytic model is presented for evaluating the decrement in impulse due to wall effects in millimeter-scale solid propellant driven thrusters. The model assumes a thin flame sheet moving with constant velocity along the thruster axis. Both frontend ignition (FEI) and backend ignition (BEI) are considered. The decrement in impulse due to plenum heat loss and the nozzle wall boundary layer is evaluated as a function of thruster geometric scale r and a flame speed parameter $V_f = t_p/t_s$, where t_s and t_p are characteristic times for steady-state flame propagation and for pulsed flow operation, respectively. For the case of deflagration waves ($V_f \ll 1$), the plenum heat loss in BEI devices and the nozzle boundary layer loss in FEI devices vary as $(rV_f)^{-1/2}$. Thus, relatively large flame speeds are needed in millimeter-scale thrusters to avoid significant impulse loss. In a numerical example, three out of six prospective high flame speed propellants had losses of about 10% or less. Hence, millimeter-scale thrusters appear viable with regard to wall loss. However, experimental confirmation of fabrication techniques, ignition techniques, and propellant performance is needed.

Nomenclature

A = area
a = speed of sound
B = function of γ; Eq. (5)
C = constant relating to heat transfer; Eq. (31)
C_h = enthalpy loss correction to impulse; Eq. (26)
C_M = exit Mach number correction to impulse; Eq. (24)
c_p, c_v = specific heats
E = energy released by flame sheet
F = thrust
$F(V_f)$ = plenum heat transfer correction to account for V_f unequal to ∞; Eqs. (40) and (41)
F_θ = Mach number dependence of θ_e; Eq. (29b)
h = enthalpy
I = impulse
I_p = impulse generated by pulsed flow through nozzle
I_s = impulse generated by steady-state flow through nozzle
k = thermal conductivity
L_c = plenum length
M = Mach number
$\bar{m}$ = exponent $\mu \sim T^{\bar{m}}$, $k \sim T^{\bar{m}}$
Pr = Prandtl number, $\mu c_p/k$
p = pressure
$p_{0,m}$ = maximum plenum pressure
Q = net heat loss; Eq. (37)
q_w = heat flux at wall
r = radius
s = length along nozzle surface
T = temperature
T_m = mean temperature
t = time
t_p = characteristic pulse time; Eq. (4)
t_s = flame steady-state propagation time, L_c/v_f
u = velocity
V_c = plenum volume
V_f = flame speed parameter; Eq. (6a)
$V_{f,m}$ = maximum value of V_f
v_f = flame speed
W = wall thickness
x = axial distance
α = thermal diffusivity, $k/\rho c_p$
γ = ratio of specific heat, c_p/c_v
δ = thermal-layer thickness
θ = boundary-layer momentum defect thickness
μ = viscosity
ρ = density
ρ_f = initial propellant density
τ = elapsed time at given station
ϕ_1, ϕ_2 = wall temperature increase parameters

Subscripts

c = plenum geometry
e = exit section
f = flame sheet or solid propellant fuel property
g = gas property
m = evaluated at mean temperature, T_m
t = throat section
w = wall property
0 = plenum gas condition

Introduction

THE feasibility of small-scale, for example, ~1-kg net mass, satellites is currently under study.[1] These satellites require millimeter-scale thrusters for attitude control. Potential thruster systems include electrical, cold gas, or an array of small-scale solid propellant driven rockets.

In the case of millimeter-scale solid propellant driven thrusters, the ratio of surface area to volume is large. Hence, unlike conventional rockets, plenum heat transfer and nozzle boundary-layer growth can severely degrade thruster impulse. The successful development of an efficient millimeter-scale thruster requires an understanding of the dependence of this impulse degradation on thruster geometry and flame speed parameters. The present study is a first attempt to define this relationship. A simple analytic model is developed that characterizes the impulse loss associated with wall effects in small-scale thrusters for cases where the boundary layers are thin but not negligible.

The present analytic study is part of a general program to develop solid propellant driven millimeter-scale thrusters.[2] Initial results relating to fabrication, ignition, and impulse measurement are reported in Ref. 3 and are briefly discussed here in the "Concluding Remarks."

Received 8 June 1998; revision received 13 May 1999; accepted for publication 17 May 1999.

*Principal Scientist, Mechanics and Materials Technology Center, 2350 E. El Segundo Boulevard. Fellow AIAA.

Theory

We consider a solid propellant driven thruster with axial flame propagation. Both frontend ignition (FEI) and backend ignition (BEI) are considered (Fig. 1). The purpose of the optional diaphragm in Fig. 1a is to prevent fuel loss in BEI devices or to aid in ignition initiation in FEI devices. It is assumed that diaphragm rupture occurs at the start and at the end of the combustion process for FEI and BEI configurations, respectively. The diaphragm, therefore, plays no role in the present fluid dynamic analysis of thruster performance. We further assume steady-state flame sheet propagation, a flame sheet thickness small with respect to combustion chamber length L_c, and an isentropic expansion of an ideal plenum gas. The results are expected to properly characterize the flow in small-scale thrusters.

In the following sections, plenum conditions are evaluated, as a function of flame speed v_f for both BEI and FEI. Ideal thrust and impulse are determined. The decrement in impulse due to heat loss in the plenum and momentum loss in the nozzle wall boundary layer is evaluated assuming thin boundary layers. The increase in plenum wall surface temperature is noted. Finally, numerical results for an example millimeter-scale thruster are discussed.

Plenum Conditions

Plenum gas properties are evaluated for both BEI and FEI.

BEI (Figure 1b)

The flame sheet is assumed to move with uniform velocity v_f. Plenum conditions are found as follows. Fluid velocity is zero due to the rear wall:

$$u_0 = 0 \tag{1a}$$

Conservation of mass indicates

$$\rho_0 = \rho_f \tag{1b}$$

where ρ_f is the initial solid propellant density. Consideration of energy conservation in flame fixed coordinates indicates

$$T_0 = (\Delta E/c_p)[1 + 0(h_f/\Delta E)] \tag{1c}$$

where ΔE is the energy release per unit mass at the flame sheet and h_f is the solid propellant enthalpy, exclusive of ΔE. Finally, the gas law $p = \rho RT$ indicates

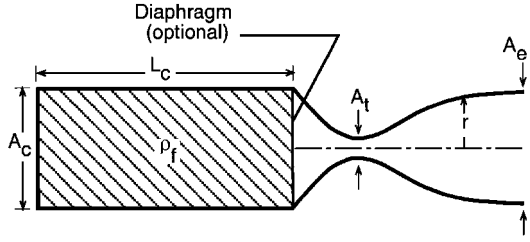

a) Preignition

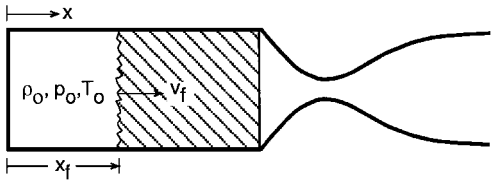

b) BEI

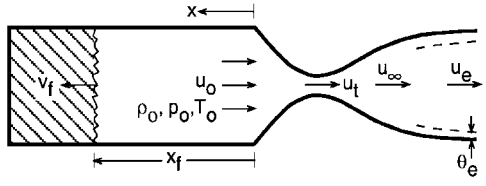

c) FEI

Fig. 1 Solid propellant driven thruster.

$$p_0 = R(\rho_f \Delta E/c_p)[1 + 0(h_f/\Delta E)] \equiv p_{0,m} \tag{1d}$$

Equation (1d) defines $p_{0,m}$, which is the maximum pressure encountered for either BEI or FEI. The time required for the flame sheet to traverse the combustion chamber is t_s and equals

$$t_s = L_c/v_f \tag{1e}$$

Plenum conditions are steady state for $t \le t_s$. Plenum conditions are unsteady for $t > t_s$, due to flow expansion through the nozzle.

The variation of plenum properties with time, for $t > t_s$, is now determined. For present purposes, we now measure time from the start of the expansion and neglect the contribution of the nozzle entrance region to plenum volume. Let $p_0(0)$ denote the pressure at the start of the expansion ($t = 0$) and let $p_0(t)$ denote pressure at a subsequent time, with similar notations for the other variables. Equating the rate of plenum gas loss to the mass flow rate at the nozzle throat indicates

$$\frac{\mathrm{d}\rho_0 V_c}{\mathrm{d}t} = -\rho_t a_t A_t \tag{2}$$

Integration of Eq. (2), with the assumption of isentropic flow yields

$$\frac{\rho_0(t)}{\rho_0(0)} = \left[\frac{p_0(t)}{p_0(0)}\right]^{1/\gamma} = \left[\frac{T_0(t)}{T_0(0)}\right]^{1/(\gamma-1)} = \left[\frac{a_0(t)}{a_0(0)}\right]^{2/(\gamma-1)}$$
$$= \left(1 + \frac{\gamma - 1}{2}\frac{t}{t_p}\right)^{-2/(\gamma-1)} \tag{3}$$

where t_p is the characteristic pulse (discharge) time defined by

$$t_p = \frac{V_c}{B a_0(0) A_t} \tag{4}$$

$$B = \rho_t a_t/\rho_0 a_0 = [2/(\gamma+1)]^{(\gamma+1)/[2(\gamma-1)]} = 0.5787 \qquad \left(\gamma = \tfrac{7}{5}\right) \tag{5}$$

Here t_p is the time it would take to exhaust the plenum mass if the plenum conditions remained constant. We define

$$V_f \equiv (1/B)(v_f/a_0)(A_c/A_t) \tag{6a}$$

and observe

$$t_p/t_s = V_f \tag{6b}$$

Thus, V_f can be interpreted either as a normalized flame speed or as the ratio of t_p/t_s. The limits $V_f \to 0$ and ∞ correspond to essentially steady-state and essentially pulse operation, respectively.

We note, for later reference, isentropic flow relations for the nozzle. Local Mach number M is related to the local area A by

$$A/A_t = (B/M)\{1 + [(\gamma-1)/2]M^2\}^{(\gamma+1)/[2(\gamma-1)]} \tag{7a}$$

Flow properties at A are related to plenum conditions by

$$T/T_0 = (p/p_0)^{(\gamma-1)/\gamma} = (\rho/\rho_0)^{\gamma-1} = (a/a_0)^2$$
$$= \{1 + [(\gamma-1)/2]M^2\}^{-1} \tag{7b}$$

FEI (Figure 1c)

Plenum conditions, for the case of FEI, are now defined. Mass conservation indicates

$$\frac{\mathrm{d}(\rho_0 x_f)}{\mathrm{d}t} = \rho_f v_f - \rho_t a_t \frac{A_t}{A_c} \tag{8}$$

For steady-state flame propagation, $v_f = \mathrm{d}x_f/\mathrm{d}t = \text{const}$, Eq. (8) becomes

$$V_f = \frac{\rho_0/\rho_f}{1 - (\rho_0/\rho_f)} \tag{9}$$

or equivalently

$$\rho_0/\rho_f = V_f/(1+V_f) \tag{10}$$

Equations (9) and (10) apply for FEI only. (Recall, $\rho_0/\rho_f = 1$, $0 \le V_f \le \infty$ for BEI.) Consideration of the energy equation, in flame fixed coordinates, indicates

$$T_0 = (\Delta E/c_p)\left\{1 + 0(h_f/\Delta E) + 0\left(M_0^2\right) + 0[M_0(v_f/a_0)]\right\} \tag{11}$$

The plenum temperature T_0 is the same as for the BEI case provided $M_0 \ll 1$, which can be assured by $A_t \ll A_c$. The gas law $p_0 = R\rho_0 T_0$ indicates

$$p_0/p_{0,m} = (\rho_0/\rho_f)\left\{1 + 0(h_f/\Delta E) + 0\left(M_0^2\right) + 0[M_0(v_f/a_0)]\right\} \tag{12}$$

where $p_{0,m}$ is the pressure associated with BEI [Eq. (1d)] and is the maximum possible pressure for FEI. Thus, ρ_0/ρ_f and $p_0/p_{0,m}$ are essentially equal. For $t > t_s$, we again have pulsed operation. Equation (6b), $t_p/t_s = V_f$, continues to apply.

Evaluation of V_f

The evaluation of the flame speed parameter V_f is discussed for cases where $V_f \gg 1$ and for deflagrations.

Case $V_f \gg 1$

The condition

$$V_f \gg 1 \tag{13}$$

corresponds to cases where the combustion time t_s is small relative to the pulse time t_p. This can occur when either the combustion is fast, that is, high flame speed propellants, electrically augmented combustion, etc., or the nozzle throat area is relatively small, that is, large t_p. In this limit, the details of the combustion process are unimportant.

Deflagration Case

For the case of a deflagration, the variation of flame speed v_f (in centimeters per second) with pressure p_0 (in atmosphere, standard) is generally expressed in the form

$$v_f = v_r(p_0)^n \tag{14}$$

where v_r is the flame speed at 1 atm and n is a constant. Values for v_r and n are given later. Define

$$V_{f,m} = (1/B)(A_c/A_t)(v_r/a_0)p_{0,m}^n \tag{15}$$

That is, $V_{f,m}$ is the value of V_f that corresponds to $p_0 = p_{0,m}$. For BEI

$$V_f = V_{f,m} \tag{16}$$

For FEI, V_f is found from $V_f/V_{f,m} = (\rho_0/\rho_f)^n$ or

$$(1+V_f)^n V_f^{1-n} = V_{f,m} \tag{17a}$$

A numerical evaluation of V_f, for given $V_{f,m}$, is generally required. Limiting cases are as follows.

For $V_{f,m}^{1/(1-n)} \ll 1$:

$$V_f = V_{f,m}^{1/(1-n)}\left\{1 - [n/(1-n)]V_{f,m}^{1/(1-n)}\right\}\left[1 + 0\left(V_f^2\right)\right] \tag{17b}$$

For $V_{f,m} \gg 1$:

$$V_f = V_{f,m} - n + 0(1/V_{f,m}) \tag{17c}$$

For $n = 1$:

$$V_f = 0, \qquad 0 \le V_{f,m} \le 1 \tag{17d}$$

$$V_f = V_{f,m} - 1, \qquad 1 \le V_{f,m} \tag{17e}$$

The values of v_r and n, for use in Eq. (14), are generally defined from experimental plots of v_f vs p_0 and apply for a restricted range of p_0. For example, Fig. 10-5 in Ref. 4 indicates that, for $20 \le p_0 \le 200$, ammonium nitrate has the values

$$v_r = 0.04, \qquad n = 0.45 \tag{18a}$$

and asphalt perchlorate has the values

$$v_r = 0.12, \qquad n = 0.73 \tag{18b}$$

The value of n generally increases with increase in pressure. The variation of v_f with p_0 for four double-base propellants is given in Fig. 2, which is reproduced from Ref. 5. These curves are correlated to within 10% by the values, for propellant 1

$$v_r = 0.027, \qquad n = 0.75 \tag{18c}$$

for propellant 2

$$v_r = 0.052, \qquad n = 0.72 \tag{18d}$$

for propellant 3

$$v_r = 0.10, \qquad n = 0.65 \tag{18e}$$

and for propellant 4

$$v_r = 0.11, \qquad n = 0.78 \tag{18f}$$

for $10 \le p_0$, atm $\le 10^3$. The exponent n increases to values of 0.95 and 0.90 at pressures of order 10^3 atm for propellants 1 and 2, respectively.

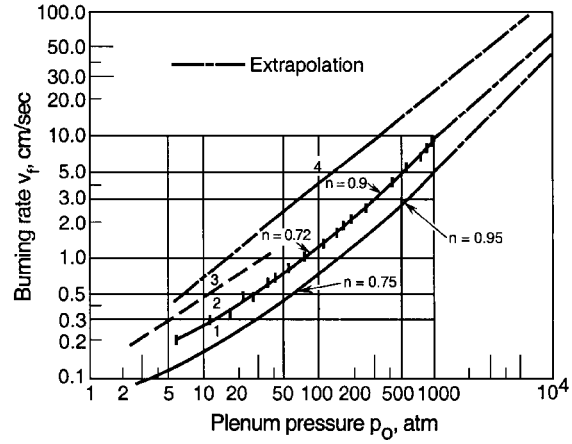

Fig. 2 Burning rate laws of control double-base propellants: 1, "cool" propellant, 820 cal/g; 2, "hot" propellant, 1100 cal/g; 3, "hot" propellant, 1320 cal/g; and 4, pure nitroglycerin, 1770 cal/g.

The unextrapolated portions of the curves in Fig. 2 are from Fig. 2 of Ref. 5. The propellant material is nitroglycerin plus nitrocellulose plus a stabilizer. The energetic level of the propellant depends on the relative amounts of nitroglycerin and nitrocellulose.

Extrapolation of the curves in Fig. 2 indicates $v_f \approx 100$ cm/s at $p_0 = 10^4$ atm. The corresponding value of $V_{f,m}$ is

$$V_{f,m} = 0(10^{-1}) \tag{19}$$

where the values $v_f = 100$ cm/s, $a_0 = 10^5$ cm/s, and $A_c/A_t = 100$ have been used. Thus $V_{f,m}$ is small for deflagration waves, and Eq. (17b) can be used to evaluate V_f.

Thrust and Impulse

We now evaluate the thrust and impulse of the configurations in Fig. 1. Let subscript e denote freestream conditions at the nozzle exit. Consideration of the flux of momentum at the exit leads to a thrust force

$$F = \int (\rho u^2 + p)_e \, dA_e \tag{20a}$$

$$F = \rho_e u_e^2[1 - (2\theta_e/r_e)]A_e + p_e A_e \tag{20b}$$

where

$$\theta_e = \int_0^{r_e} \left(1 - \frac{\rho u^2}{\rho_e u_e^2}\right) \frac{r}{r_e}\, \mathrm{d}r \tag{20c}$$

Here p_e, ρ_e, and u_e denote freestream conditions, r_e is the nozzle exit radius, and θ_e is a momentum defect thickness. In the present case of a relatively thin boundary layer, Eq. (20c) reduces to the conventional expression for boundary-layer momentum defect thickness at the nozzle exit. It can be shown then the effect of the displacement thickness parameter $2\delta^*/r_e$ on thrust is of order $(2\delta^*/r_e)^2$ and is neglected herein. An alternate form for Eq. (20) is

$$F/A_e = \rho_e u_e^2 \left[1 + \left(1/\gamma M_e^2\right)\right] - \rho_e u_e^2 (2\theta_e/r_e) \tag{21}$$

The corresponding impulse is

$$\frac{I}{A_e} = \int_0^\infty \frac{F}{A_e}\, \mathrm{d}t = \left(1 + \frac{1}{\gamma M_e^2}\right) \int_0^\infty \rho_e u_e^2\, \mathrm{d}t - \int_0^\infty \frac{2\theta_e}{r_e} \rho_e u_e^2\, \mathrm{d}t \tag{22}$$

where, for $\mu \sim T$ and fixed propellant and geometry, $\theta_e \sim T_e^{3/4}/P_e^{1/2}$ [see Eq. (28)]. The integration is conducted separately for pulsed and for steady-state operation. We consider BEI and FEI separately.

BEI

Let I_p be the net impulse generated by the pulsed flow. Substitution of Eqs. (3) and (28) into Eq. (22) yields, for $\mu \sim T$,

$$\frac{1}{C_M} \frac{I_p}{\rho_f V_c \sqrt{2h_0}} = \frac{2}{\gamma + 1} \left[1 - \frac{2\theta_e}{r_e} \frac{2(\gamma + 1)/(3\gamma - 1)}{1 + \left(\gamma M_e^2\right)^{-1}}\right] \tag{23}$$

where

$$C_M = \left(1 + \frac{1}{\gamma M_e^2}\right) \Bigg/ \left(1 + \frac{2}{\gamma - 1} \frac{1}{M_e^2}\right)^{\frac{1}{2}} \tag{24a}$$

$$C_M = 1 - \frac{1}{\gamma(\gamma - 1)} \frac{1}{M_e^2} + 0\left(\frac{1}{M_e^4}\right) \tag{24b}$$

$$C_M = \frac{(\gamma^2 - 1)^{\frac{1}{2}}}{\gamma} \qquad (M_e = 1) \tag{24c}$$

Here $I_p/[\rho_f V_c \sqrt{(2h_0)}]$ is the ratio of impulse to the value corresponding to a steady-state expansion to a vacuum. The factor C_M corrects the impulse for expansion to a finite value of M_e. The factor $2/(\gamma + 1)$ in Eq. (23) is less than 1 because of the reduction in plenum enthalpy during the unsteady expansion. The term involving θ_e gives the reduction in impulse due to the momentum loss in the nozzle boundary layer.

FEI

Let I_s be the impulse generated during the steady-state flow. In this case the integrands are constant in Eq. (22). The net mass expelled is $(\rho_f - \rho_0)V_c$. Equation (22) then yields

$$\frac{1}{C_M} \frac{I_s}{\rho_f V_c \sqrt{2h_0}} = \left(1 - \frac{\rho_0}{\rho_f}\right) \left[1 - \frac{2\theta_e}{r_e} \frac{1}{1 + \left(\gamma M_e^2\right)^{-1}}\right] \tag{25a}$$

The mass expelled during the unsteady expansion is $\rho_0 V_c$. The corresponding impulse is then

$$\frac{1}{C_M} \frac{I_p}{\rho_f V_c \sqrt{2h_0}} = \frac{2}{\gamma + 1} \frac{\rho_0}{\rho_f} \left[1 - \frac{2\theta_e}{r_e} \frac{2(\gamma + 1)/(3\gamma - 1)}{1 + \left(\gamma M_e^2\right)^{-1}}\right] \tag{25b}$$

The net impulse is the sum of Eqs. (25a) and (25b).

Effect of Plenum Heat Transfer on Impulse

The preceding expressions for impulse neglect the effect of heat loss in the plenum. The proper correction for this effect is to determine the enthalpy of each gas particle as it enters the nozzle. A simpler but less accurate approach is to use an average enthalpy for the mass that exits the plenum. Let Δh_0 represent the average plenum enthalpy loss. The impulse is then found by multiplying the preceding expressions by

$$C_h = \sqrt{1 - (\Delta h_0/h_0)} = 1 - \tfrac{1}{2}(\Delta h_0/h_0) + 0(\Delta h_0/h_0)^2 \tag{26}$$

That is, C_M in Eqs. (23) and (25) is replaced by the product $C_M C_h$.

Nozzle Boundary Layer

Exit section momentum defect thickness and the corresponding impulse loss are estimated in the following section. It is assumed that the boundary-layer thickness is small relative to the local nozzle radius r.

The momentum defect thickness at the exit section can be expressed[6] as

$$\theta_e = \frac{0.664}{\rho_e u_e r_e} \left(\int_0^{s_e} \rho_m \mu_m u_\infty r^2\, \mathrm{d}s\right)^{\frac{1}{2}} \tag{27a}$$

where ρ_m and μ_m are evaluated at a mean temperature given by

$$T_m/T_e = \tfrac{1}{2}[1 + (T_w/T_e)] + 0.11(\gamma - 1) P_r^{\frac{1}{2}} M_e^2 \tag{27b}$$

where $Pr = 0.72$ for air. The quantities u_∞ and s denote local freestream velocity and distance along the nozzle surface, respectively. An approximate expression for θ_e can be obtained by neglecting the variation of $\rho_m \mu_m u_\infty$ and assuming r to be proportional to s. By assuming $\mu \sim T^{\bar{m}}$, we have the result

$$\frac{\theta_e}{r_e} = \frac{0.664}{\sqrt{3}} \sqrt{\frac{\mu_e}{\rho_e u_e} \frac{s_e/r_e}{r_e}} \left(\frac{T_e}{T_m}\right)^{(1 - \bar{m})/2} \tag{28}$$

where r_e/s_e is approximately equal to the nozzle half-angle. The effect of Mach number, geometric scale, and flame speed can be displayed by writing Eq. (28) in the form

$$\frac{\theta_e}{r_e} = \frac{0.664}{\sqrt{3}} \sqrt{\frac{\mu_0}{\rho_f a_0} \frac{s_e/r_e}{r_e}} \left(\frac{T_e}{T_m}\right)^{(1 - \bar{m})/2} \left(\frac{\rho_f}{\rho_0}\right)^{\frac{1}{2}} F_\theta \tag{29a}$$

where

$$F_\theta = \left\{1 + [(\gamma - 1)/2] M_e^2\right\}^{(1 - \bar{m})/2 + (3 - \gamma)/[4(\gamma - 1)]} \Big/ M_e^{\frac{1}{2}} \tag{29b}$$

and isentropic flow is assumed. The corresponding displacement thickness δ^* can be estimated from[7]

$$\delta^*/\theta_e = 2.61$$

The impulse loss due to the nozzle wall boundary layer is found by substituting Eq. (29a) into Eqs. (23) and (25). Neglecting the effect of M_e, the impulse loss for BEI is of order

$$\frac{2\theta_e}{r_e} = 0\left[\left(\frac{\mu_0}{\rho_f a_0} \frac{1}{r_e}\right)^{\frac{1}{2}}\right] \tag{30a}$$

and for FEI is of order

$$\frac{2\theta_e}{r_e} = 0\left[\left(\frac{\mu_0}{\rho_f a_0} \frac{1}{r_e} \frac{1 + V_f}{V_f}\right)^{\frac{1}{2}}\right] \tag{30b}$$

The impulse loss varies inversely with the square root of the geometric scale. The effect of V_f is significant only in the case of FEI and $V_f \ll 1$, wherein the impulse loss varies as $(r_e V_f)^{-1/2}$. In the latter case, V_f must be increased as r_e is decreased to maintain a small impulse loss.

Heat Loss in Plenum

It is assumed that the thermal-layer thickness is small in relation to the plenum radius r_c. The heat flux at the plenum wall can then be expressed, for fixed T_0 and T_w, as

$$\frac{q_w}{\rho_m c_p (T_0 - T_w)} = C\sqrt{\frac{\alpha_m}{\tau}} \tag{31}$$

where C is a weak function of ρ_0/ρ_f and

$$\tau = t - x/v_f \tag{32}$$

That is, at each section x, τ represents the time that has elapsed since passage of the flame sheet. For BEI,

$$C = 1/\sqrt{\pi} \tag{33}$$

which corresponds to conduction in the absence of convection.[8] For FEI, the coefficient C is found from[9]

$$C = 0.332[1 + 1.888(\rho_0/\rho_f)]^{\frac{1}{2}} \tag{34a}$$

Limiting values are

$$0.332 \le C \le 1/\sqrt{\pi} \tag{34b}$$

for

$$0 \le \rho_0/\rho_f \le 1 \tag{34c}$$

The value $C = 0.332$ corresponds to steady-state flow of a fluid, with $Pr = 1$, over a semi-infinite plate.[9] Equation (31) is exact for the period of steady-state operation ($t \le t_s$) and for primarily pulsed operation ($t_s/t_p \ll 1$) and is approximately valid for all cases.

Assume that the pulsed operation is characterized by the initial plenum conditions and a pulse length of t_p. The net period of disturbed flow at each section x is then

$$\tau = (t_s - x/v_f) + t_p \tag{35}$$

The net amount of heat transferred into the wall, at station x, is denoted by $Q(x)$ and is found by integrating Eq. (31) with respect to τ, using Eq. (35) as an upper limit. The result is

$$\frac{Q(x)}{\rho_m c_p (T_0 - T_w)} = 2C\left[\alpha_m\left(t_s + t_p - \frac{x}{v_f}\right)\right]^{\frac{1}{2}} \tag{36}$$

The net loss of heat Q is found by integrating over the plenum surface area

$$Q = 2\pi r_c \int_0^{L_c} Q(x)\,dx \tag{37}$$

The result is

$$\frac{Q}{\rho_m c_p (T_0 - T_w) V_c} = \frac{8}{3}\frac{C}{r_c}(\alpha_m t_p)^{\frac{1}{2}}\frac{t_p}{t_s}\left[\left(\frac{t_s}{t_p} + 1\right)^{\frac{3}{2}} - 1\right] \tag{38}$$

Equation (38) becomes, for $k \sim T^{\bar{m}}$,

$$\frac{Q}{\rho_f c_p (T_0 - T_w) V_c} = \frac{4}{\pi^{\frac{1}{2}}}\frac{1}{r_c}\left(\frac{k_0 t_p}{\rho_f c_p}\right)^{\frac{1}{2}}\left(\frac{T_0}{T_m}\right)^{(1-\bar{m})/2} F(V_f) \tag{39}$$

where, for BEI,

$$F(V_f) = \tfrac{2}{3}\left[(1 + V_f)^{\frac{3}{2}} - V_f^{\frac{3}{2}}\right]\Big/(V_f)^{\frac{1}{2}} \tag{40a}$$

$$F(V_f) = \tfrac{2}{3}(V_f)^{-\frac{1}{2}}, \qquad V_f \to 0 \tag{40b}$$

$$F(V_f) = 1, \qquad V_f \to \infty \tag{40c}$$

and for FEI

$$F(V_f) = 0.392(1 + 2.888V_f)^{\frac{1}{2}}\left[(1 + V_f)^{\frac{3}{2}} - V_f^{\frac{3}{2}}\right]\Big/(1 + V_f) \tag{41a}$$

$$F(V_f) = 0.392, \qquad V_f \to 0 \tag{41b}$$

$$F(V_f) = 1, \qquad V_f \to \infty \tag{41c}$$

Equation (39) has been normalized to the value for $V_f \to \infty$, that is, $F(\infty) = 1$. For BEI, $Q \to \infty$ as $V_f \to 0$, due to the increase in residence time. It is somewhat surprising to see that Q is relatively insensitive to V_f for FEI and, in fact, decreases as V_f decreases. The insensitivity of Q to V_f is a consequence of an inverse relation between residence time and heat transfer rate.

The average heat loss per unit mass from the plenum gas is found from

$$\frac{\Delta h_0}{h_0} = \frac{Q}{\rho_f c_p T_0 V_c} \tag{42a}$$

$$\frac{\Delta h_0}{h_0} = \left[\frac{Q}{\rho_f c_p (T_0 - T_w) V_c}\right]\left(1 - \frac{T_w}{T_0}\right) \tag{42b}$$

The assumption of a thin thermal layer is valid when $\Delta h_0/h_0 \ll 1$. The latter condition is violated for BEI in the limit $V_f \to 0$.

The decrement in impulse due to plenum heat transfer is found by substituting Eqs. (39) and (42) into Eq. (26). The loss is of order

$$\tfrac{1}{2}(\Delta h_0/h_0) = \mathcal{O}\left\{[(\mu_0/\rho_f a_0)(L_c/A_t)]^{\frac{1}{2}} F(V_f)\right\} \tag{43a}$$

As in the case of the nozzle boundary layer, the impulse loss varies inversely with the square root of the geometric scale, A_t/L_c. The effect of V_f is significant only in the case of BEI and $V_f \ll 1$. In this case, Eq. (43a) becomes

$$\tfrac{1}{2}(\Delta h_0/h_0) = \mathcal{O}\left\{[(\mu_0/\rho_f a_0)(L_c/A_t)(1/V_f)]^{\frac{1}{2}}\right\} \tag{43b}$$

wherein the impulse loss varies as $(V_f A_t/L_c)^{-1/2}$. The latter result is similar to the impulse loss due to the nozzle boundary layer in the case of FEI and $V_f \ll 1$, for example, Eq. (30b). Here, the characteristic length is A_t/L_c. Hence, V_f must be increased, as geometric scale is decreased, to maintain low impulse loss in BEI, $V_f \ll 1$ thrusters.

Plenum Surface Temperature

The variation of plenum surface temperature with time is of interest and is evaluated herein.

The local thermal boundary-layer thickness in the gas, δ_g, and wall, δ_w, can be estimated from

$$\delta_g = (2/C_g)\sqrt{\alpha_g \tau} \tag{44a}$$

$$\delta_w = (2/C_w)\sqrt{\alpha_w \tau} \tag{44b}$$

where mean values of α are assumed. The corresponding heat flux at the wall, assuming a parabolic temperature profile (where T_w is wall surface temperature and $T_{w,i}$ is initial wall temperature), is then

$$q_w = \frac{C_g k_g (T_0 - T_w)}{\sqrt{\alpha_g \tau}} = \frac{C_w k_w (T_w - T_{w,i})}{\sqrt{\alpha_w \tau}} \tag{45}$$

where $C_g = C_w = 1/\sqrt{\pi}$ for agreement with an exact solution of the conduction equation.[8] Equations (44) and (45) assume that the thermal thickness in the gas and wall is small compared with the gas and wall thickness, respectively. Equation (45) indicates

$$\frac{T_w - T_{w,i}}{T_0 - T_{w,i}} = \frac{\phi_1\sqrt{\rho_0/\rho_f}}{1 + \phi_1\sqrt{\rho_0/\rho_f}} \tag{46a}$$

where

$$\phi_1 = \left[\frac{\rho_f (c_p k_0)_g}{(\rho c_p k)_w}\right]^{\frac{1}{2}} \tag{46b}$$

For $\phi_1 \ll 1$ and $T_{w,i}/T_0 \ll 1$, Eq. (46b) becomes

$$\frac{T_w - T_{w,i}}{T_0} = \phi_1\sqrt{\frac{\rho_0}{\rho_f}} \tag{46c}$$

which is generally applicable.

If the wall thickness W is small compared with δ_w as defined in Eq. (44b), the wall temperature is found from

$$\frac{T_w - T_{w,i}}{T_0 - T_{w,i}} = 1 - \exp\left[-\phi_2\left(\frac{\rho_0}{\rho_f}\right)^{\frac{1}{2}}\left(\frac{\tau}{t_p}\right)^{\frac{1}{2}}\right] \tag{47a}$$

where

$$\phi_2 = \frac{2}{\pi^{\frac{1}{2}}}\frac{[\rho_f (c_p k_0)_g t_p]^{\frac{1}{2}}}{W(\rho c_p)_w} \tag{47b}$$

Equation (47b) assumes that the temperature is uniform within the wall and that the rear surface of the wall is insulated. The maximum wall temperature occurs at $x = 0$, $\tau = t_s + t_p$ and equals, for BEI,

$$\frac{T_w - T_{w,i}}{T_0 - T_{w,i}} = 1 - \exp\left[-\phi_2\left(1 + V_f^{-1}\right)^{\frac{1}{2}}\right] \tag{48}$$

and for FEI

$$\frac{T_w - T_{w,i}}{T_0 - T_{w,i}} = 1 - \exp(-\phi_2) \tag{49}$$

Numerical Example

We evaluate the effect of the flame speed parameter V_f on the performance of a millimeter-scale thruster with airlike and aluminum-like plenum gas and wall properties, respectively (see Appendix for gas and wall properties). The following geometry conditions are assumed:

$$r_c = r_e = 10 r_t = 0.05\,\text{cm}, \qquad L_c = 1.0\,\text{cm}$$

$$V_c = 7.854 \times 10^{-3}\,\text{cm}^3, \qquad r_e/s_e = 0.25 \tag{50a}$$

the plenum conditions are

$$\rho_f = 1\,\text{g/cm}^3, \qquad T_0 = 3000\,\text{K} \tag{50b}$$

and the exit condition is

$$M_e = 6.94 \tag{50c}$$

The nominal impulse and pulse time are

$$\rho_f V_c \sqrt{2h_0} = 1930\,\text{dyne} \cdot \text{s} \tag{51a}$$

$$t_p = 1.573 \times 10^{-3}\,\text{s} \tag{51b}$$

Plenum wall temperature parameters are

$$\phi_1 = 1.786 \times 10^{-2} \tag{51c}$$

$$\phi_2 = \frac{7.425 \times 10^{-3}}{W(\text{cm})/0.1} \tag{51d}$$

Thruster performance is as follows.

BEI

$$p_0 = p_{0,m} = 8517\,\text{atm} \tag{52a}$$

$$\rho_0/\rho_f = 1 \tag{52b}$$

$$2\theta_e/r_e = 2.722 \times 10^{-3} \qquad (\bar{m} = 1) \tag{52c}$$

$$\tfrac{1}{2}(\Delta h_0/h_0) = 3.437 \times 10^{-2} F(V_f) \qquad (\bar{m} = 1) \tag{52d}$$

$$\tfrac{1}{2}(\Delta h_0/h_0) = 3.437 \times 10^{-2}, \qquad V_f \gg 1 \tag{52e}$$

$$\tfrac{1}{2}(\Delta h_0/h_0) = 2.292 \times 10^{-2}/\sqrt{V_f}, \qquad V_f \ll 1 \tag{52f}$$

$$\tfrac{1}{2}(\Delta h_0/h_0) < 0.1, \qquad V_f > 0.052 \tag{52g}$$

For a thick wall

$$\frac{T_w - T_{w,i}}{T_0 - T_{w,i}} = \frac{\phi_1}{1 + \phi_1} \tag{52h}$$

For a thin wall

$$\frac{T_w - T_{w,i}}{T_0 - T_{w,i}} = 1 - \exp\left[-\phi_2\left(\frac{1 + V_f}{V_f}\right)^{\frac{1}{2}}\right] \tag{52i}$$

It follows that for a thick wall

$$T_w - T_{w,i} = 53\,\text{K} \tag{52j}$$

and for a thin wall

$$T_w - T_{w,i} = \frac{22}{W/0.1}\,\text{K}, \qquad V_f \gg 1 \tag{52k}$$

$$T_w - T_{w,i} < \frac{98}{W/0.1}\,\text{K}, \qquad V_f > 0.052 \tag{52l}$$

Thus, for BEI, the plenum pressure is high and the boundary-layer momentum loss is low. The thermal loss and the corresponding thin wall temperature become large as $V_f \to 0$. The thermal loss parameter $\Delta h_0/(2h_0)$ is less than 0.1 when $V_f > 0.052$. In the limit $V_f \gg 1$, the surface temperature rise is 53 K and $22/(W/0.1)$ K for a thick wall and a thin wall, respectively. For $V_f = 0.052$, the thin wall temperature rise is $98/(W/0.1)$ K. Thus, the major obstacles to BEI are a high plenum pressure, which may pose structural problems, and a requirement for sufficiently high V_f to avoid excessive plenum heat loss.

FEI

$$p_0 = 8517[V_f/(1 + V_f)]\,\text{atm} \tag{53a}$$

$$\rho_0/\rho_f = V_f/(1 + V_f) \tag{53b}$$

$$2\theta_e/r_e = 2.722 \times 10^{-3}[(1 + V_f)/V_f]^{\frac{1}{2}} \qquad (\bar{m} = 1) \tag{53c}$$

$$2\theta_e/r_e < 0.1, \qquad V_f > 7.4 \times 10^{-4} \tag{53d}$$

$$\tfrac{1}{2}(\Delta h_0/h_0) = 3.437 \times 10^{-2} F(V_f) \qquad (\bar{m} = 1) \tag{53e}$$

$$\tfrac{1}{2}(\Delta h_0/h_0) = 3.437 \times 10^{-2}, \qquad V_f \gg 1 \tag{53f}$$

$$\tfrac{1}{2}(\Delta h_0/h_0) = 1.347 \times 10^{-2}, \qquad V_f \ll 1 \tag{53g}$$

For a thick wall

$$\frac{T_w - T_{w,i}}{T_0 - T_{w,i}} = \frac{\phi_1(\rho_0/\rho_f)^{\frac{1}{2}}}{1 + \phi_1(\rho_0/\rho_f)^{\frac{1}{2}}} \tag{53h}$$

For a thin wall

$$\frac{T_w - T_{w,i}}{T_0 - T_{w,i}} = 1 - \exp(-\phi_2) \tag{53i}$$

It follows that for a thick wall

$$T_w - T_{w,i} \le 53\,\text{K} \tag{53j}$$

and for a thin wall

$$T_w - T_{w,i} = \frac{22}{W/0.1}\,\text{K} \tag{53k}$$

In the case of FEI, the plenum pressures associated with deflagration flame speeds, that is, $V_f \ll 1$, are low. However, the boundary-layer momentum loss is high. To achieve $2\theta_e/r_e < 0.1$, a value $V_f > 7.4 \times 10^{-4}$ is needed. The corresponding plenum pressure range is $p_0 > 6.3$ atm. The plenum enthalpy loss and the corresponding wall temperature rise are small for all V_f.

Table 1 Evaluation of impulse loss parameters $2\theta_e/r_e$ and $\Delta h_0/(2h_0)$ for example thruster

	FEI			BEI		
Propellant	V_f	p_0, atm	$2\theta_e/r_e$	V_f	p_0, atm	$\Delta h_0/2h_0$
Asphalt perchlorate	7.84×10^{-4}	6.670	0.097	0.167	8517	0.056
4	6.84×10^{-4}	5.820	0.104	0.201	8517	0.051
3	2.71×10^{-4}	2.310	0.165	0.056	8517	0.096
Ammonium nitrate	3.78×10^{-5}	0.322	0.443	0.004	8517	0.377
2	3.23×10^{-5}	0.275	0.479	0.055	8517	0.097
1	2.01×10^{-6}	0.017	0(1)	0.038	8517	0.118

Impulse Loss Associated with Equation (18) Propellants

The impulse loss parameters $2\theta_e/r_e$ and $\Delta h_0/(2h_0)$ are now evaluated for the example thruster [Eqs. (50–53)] using propellant flame speeds characterized by Eq. (18). We continue the assumption of an airlike plenum gas and ignore variations in energy release. Thus, only variations in flame speed are considered. The results are given in Table 1. The propellants are listed in order of decreasing values of V_f in the FEI region. Values of $2\theta_e/r_e$ and $\Delta h_0/(2h_0)$ of order 0.1 are consistent with the assumption of a thin boundary layer. Larger values violate the thin boundary-layer assumption and overestimate the impulse loss. It is seen that the three higher flame speed propellants have impulse (nozzle boundary layer) losses of order 0.1 for FEI devices. Five of the six propellants have impulse (plenum heat transfer) losses of order 0.1 or less for BEI devices.

Plenum pressures are included in Table 1. It is necessary to confirm that the values of v_r and n used in Eq. (14) are consistent with experimental observations of flame speed at these pressures. For FEI, the plenum pressures are relatively low and increase with V_f. In the case of BEI, the plenum pressure is a function of energy release and is high.

Asphalt perchlorate and the double-base propellants 1–4, listed in Eqs. (18), are not conventional rocket fuels. They were included in the present study because they have relatively high flame speeds, a requirement for efficient impulse generation in small-scale devices. From a practical point of view, it remains to be demonstrated that propellants of the type indicated in Eqs. (18) can, in fact, be fabricated and ignited in millimeter-scale thrusters. The present results should be viewed as an indication of the potential performance of these type of propellants.

Concluding Remarks

A simple analytic model has been developed for evaluating the decrement in impulse due to wall effects in millimeter-scale solid propellant driven thrusters. The model assumes an ideal gas, a thin flame sheet, and uniform flame speed along the thruster axis. It is believed that departures from these conditions can be accommodated by appropriate choice of fluid properties, energy release, and effective flame speed.

Thruster performance has been evaluated as a function of the flame speed parameter $V_f = t_p/t_s$. For the case of deflagrations ($V_f \ll 1$), the impulse loss due to plenum heat transfer, in BEI thrusters, and due to the nozzle wall boundary layer, in FEI thrusters, is proportional to $(rV_f)^{-1/2}$, where r is a characteristic thruster length [see Eqs. (30) and (43)]. Hence, to avoid large impulse loss, it is necessary to increase flame speed as the thruster scale r is decreased.

Millimeter-scale thrusters require relatively large flame speeds to avoid wall-induced impulse loss. Six prospective propellants are listed in Eq. (18). Computations using these propellants in a prototype millimeter-scale thruster indicated that three of the higher flame speed propellants resulted in impulse losses of about 10% or less. The corresponding values of V_f were in the range $V_f \geq 2.71 \times 10^{-4}$ and 0.056 for FEI and BEI thrusters, respectively.

The relative merits of FEI and BEI devices can be summarized as follows. BEI devices have less impulse loss due to wall boundary layers (Table 1) and are easier to ignite.[3] However, they have higher plenum pressures that could pose structural problems and that could result in fuel loss if diaphragm breakage occurs prematurely. Pressure levels in BEI devices can be reduced by use of less energetic fuels. In the case of FEI, the diaphragm can be relatively thin and can be used to aid in the initiation of ignition. Finally, it is noted that, if a diaphragm is used, the diaphragm breakage pattern should be such as not to obstruct the nozzle throat area.

Reference 3 describes the construction and electrical ignition of a millimeter-scale BEI device. Initial impulse measurements have been made. In this regard, Ref. 3 states, "Thermochemistry calculations, confirmed by the brightness of the thrust plume, have shown that only about 10% of the propellant has produced thrust. Our expectation is that this can be increased by nearly a factor of 10 with more complete combustion of the propellant." Reference 3 does not contain sufficient information concerning diaphragm breakage, nozzle configuration, and fuel properties to permit estimates of the contribution of wall effects to impulse loss.

Appendix: Nominal Gas and Wall Properties

We assume that plenum gas and wall properties can be characterized by air and aluminum properties, respectively. Note 1 atm $= 1.013 \times 10^6$ dynes/cm^2 and 1 cal $= 4.186 \times 10^7$ erg.

Air

The following properties are extrapolated from values at standard conditions ($T = 288.15$ K and $p = 1$ atm) and should be considered as approximate at elevated temperature (in degrees Kelvin) and pressure (in atmosphere, standard):

$$\text{molecular weight} = 28.96, \qquad \gamma = c_p/c_v = \tfrac{7}{5}$$

$$Pr = \mu c_p/k = 0.72$$

$$c_p = 6.960\,\text{cal/mole} \cdot \text{K} = 0.2403\,\text{cal/g} \cdot \text{K}$$

$$c_v = 4.965\,\text{cal/mole} \cdot \text{K} = 0.1714\,\text{cal/g} \cdot \text{K}$$

$$a = 1.098 \times 10^5 (T/3000)^{\frac{1}{2}}\ \text{cm/s}$$

$$\rho = 1.177 \times 10^{-4} p(3000/T)\ \text{g/cm}^3$$

$$\mu = 1.062 \times 10^{-3} (T/3000)^{0.76}\ \text{g/cm} \cdot \text{s}$$

$$k = 3.544 \times 10^{-4} (T/3000)^{0.76}\ \text{cal/cm} \cdot \text{s} \cdot \text{K}$$

$$\alpha \equiv k/(\rho c_p) = 12.53(T/3000)^{1.76}/p\ \text{cm}^2\text{/s}$$

$$h = c_p T = 720.9(T/3000)\,\text{cal/g}$$

Aluminum

$$\rho = 2.7\,\text{g/cm}^3, \qquad c_p = 0.206\,\text{cal/g} \cdot \text{K}$$

$$k = 0.48\,\text{cal/cm-s} \cdot \text{K}, \qquad \alpha = (k/\rho c_p)_w = 0.86\,\text{cm}^2\text{/s}$$

Acknowledgments

This study was funded by Defense Advanced Research Projects Agency via TRW Contract 524462BDC7. The author is indebted to Ronald B. Cohen of The Aerospace Corporation for technical discussions.

References

[1]Janson, S. W., and Helvajian, H., "Batch Fabricated Microthrusters: Initial Results," AIAA Paper 96-2988, July 1996.

[2]Stix, G., "Little Bangs," *Scientific American*, Vol. 279, No. 5, 1998, pp. 50, 51.

[3]Lewis, D. H., Jr., Janson, S. W., Cohen, R. B., and Antonsson, E. K., "Digital MicroPropulsion," 12th IEEE International Micro Electro Mechanical Systems Conf. (MEMS 99), Jan. 1999.

[4]Sutton, G. P., *Rocket Propulsion Elements*, Wiley, New York, 1963, pp. 320, 321.

[5]Lengellé, G., Bizot, A., Duterque, J., and Trubert, J. F., "Steady-State Burning of Homogeneous Propellants," *Fundamentals of Solid-Propellant Combustion*, edited by K. K. Kuo and M. Summerfield, AIAA, New York, 1984, pp. 361–407.

[6]Zoby, E. V., Moss, J. N., and Sutton, K., "Approximate Convective-Heating Equations for Hypersonic Flow," *Journal of Spacecraft and Rockets*, Vol. 18, No. 1, 1981, p. 64.

[7]Schlichting, H., *Boundary Layer Theory*, McGraw–Hill, New York, 1960, p. 242.

[8]Carslaw, H. S., and Jaeger, J. C., *Conduction of Heat in Solids*, Clarendon, Oxford, 1947, pp. 60, 75, 497.

[9]Mirels, H., "Boundary Layer Behind Shock or Thin Expansion Wave Moving Into Stationary Fluid," NACA TN3712, May 1956.

J. P. Gore
Associate Editor